

Vacuum-UV chemical physics in the gas phase using synchrotron radiation

Richard P. Tuckett

School of Chemistry, University of Birmingham, Edgbaston, Birmingham B15 2TT, UK

Introduction

Charged particles travelling in a circle at velocities close to the speed of light have the fundamental property that they emit continuous electromagnetic radiation, widely called *synchrotron radiation* (SR). Initially discovered in the 1950s by high-energy physicists and regarded as a hindrance, SR is now used worldwide by physicists, chemists and biologists for fundamental and applied research. The physics of such sources is well understood. Briefly, the total energy emitted by a charged particle is proportional to z^2E^4/m^4R^2 , where R is the radius of curvature, and m , z and E are the mass, charge and energy of the charged particle, respectively. In most SR sources the electron is used for the charged particle, because it is easy to generate and has a high z/m ratio. Nearly all the experiments described here use the Daresbury SR source, run by the Council of the Central Laboratory of the Research Councils on behalf of the UK Government.

In such "secondary generation" sources, electrons are injected into the storage ring at high energy, 2 GeV at Daresbury, where bending magnets maintain their orbit. The circumference of the Daresbury ring is *ca* 100 m. The universal SR is emitted tangentially to the circular motion of the electrons with a small horizontal angular divergence, *ca* 15 milliradians, and energy-selected photon beams can be used for experiments. A radio-frequency cavity replenishes the energy lost when SR is emitted, and bunches the electrons together. The SR is linearly polarised in the plane of the ring, but becomes circularly polar-

ised away from the horizontal plane. Ultra-high vacuum in the storage ring, *ca* 10^{-10} mbar, minimises the scattering of electrons with background gas molecules. Lifetimes of such sources are typically 8–24 hours. The Daresbury source operates in two modes: (a) multi-bunch mode where 160 electron bunches, 2 ns between bunches, are stored in the ring providing pseudo-continuous-wave radiation, and (b) single-bunch mode where only one bunch is in the ring, providing a temporal structure (pulse width *ca* 0.2 ns and repetition rate *ca* 3 MHz) for time-resolved experiments.

Thus SR is a continuous source of electromagnetic radiation covering the infrared through to the hard X-ray, and monochromators can be used to select the correct spectral region. The distribution of emitted radiation depends primarily on E via the *critical wavelength*, λ_c , which is proportional to E^{-3} . The peak of the distribution occurs at $0.42\lambda_c$. Thus, lower values of E are needed for higher λ photons, and the best sources for vacuum-UV radiation occur with $E < 1$ GeV, whereas hard X-ray sources need larger values of E , typically > 5 GeV. Other factors that affect the intensity of the photon beam at the experiment include the beam current, the distance between the experiment and the tangent to the electron orbit, and the efficiencies of the beamline components. Insertion devices, such as multi-pole wigglers or multi-period undulators, produce SR of much greater intensity. They comprise arrays of magnets of alternating polarity where the electrons oscillate periodically, SR is emitted at each "wiggle", and

coherent interference leads to amplification. Undulators provide the majority of beamlines on the latest "third-generation" sources such as Diamond, being built by the UK at the Rutherford and Appleton Laboratory and scheduled to open in 2007.

For gas-phase experiments in the vacuum-UV, defined broadly as wavelengths 50–200 nm (*ca* 6–25 eV), the monochromator is a crucial component, and much effort has gone into their design. At Daresbury, until very recently two normal-incidence monochromators have covered this wavelength range: a 1 m focal length Seya–Namioka and a 5 m McPherson with superior resolution. In the former instrument, the SR beam over-filled the entrance slit, so flux was lost. In 2004 it was replaced by a 1 m Wadsworth monochromator giving a much-enhanced flux. Since its design is novel, this monochromator is described in some detail below. Then in this article are described four experiments from my research programme over the last decade using such sources. They highlight specifically the versatility of SR in a region of the spectrum where readily tunable lasers do not exist, and, to my knowledge, could not have been performed with any other radiation source.

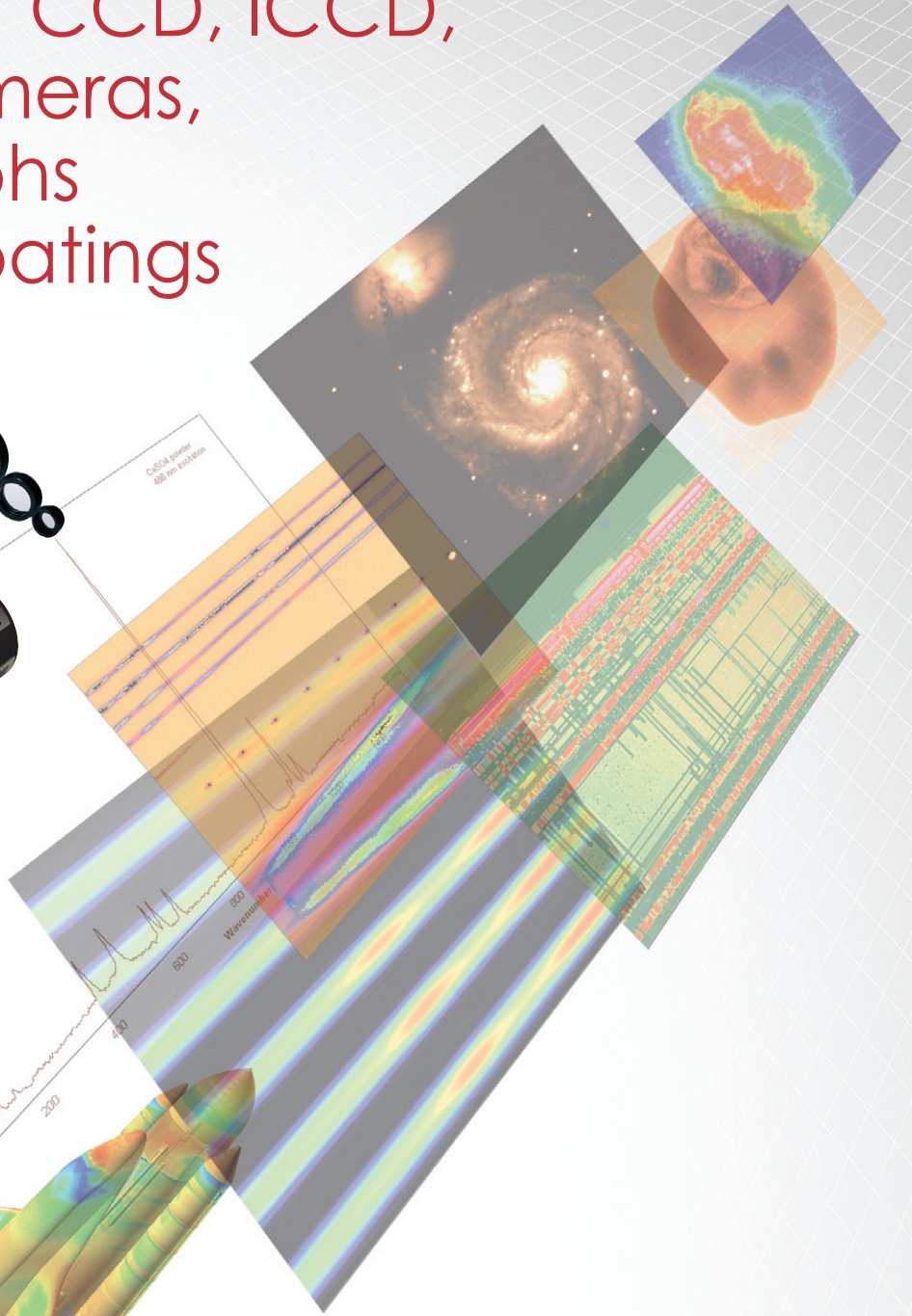
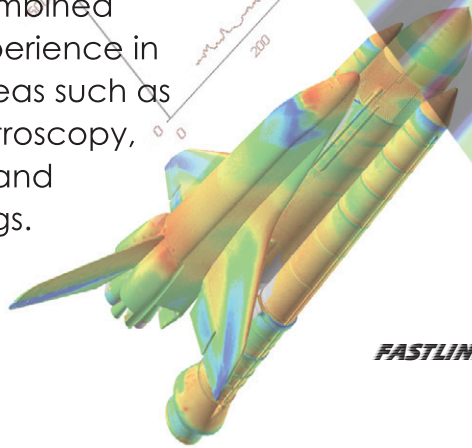
A new Wadsworth monochromator for vacuum-UV science

The Wadsworth configuration contains only one optical component, a concave diffraction grating, thus substantially reducing transmission losses. It is a great simplification over the previously-installed

The future of CCD, ICCD, EMCCD cameras, spectrographs & optical coatings



Princeton Instruments and Acton are the world's leading providers of high-performance light detection and analysis solutions. We have a combined 75 years of experience in application areas such as imaging, spectroscopy, x-ray, security and optical coatings.



FASTLINK / CIRCLE 011 FOR FURTHER INFORMATION

Call today to learn more about our sensational light detection solutions!

Princeton Instruments

ACTON

www.piacton.com

email: moreinfo@piacton.com

USA 609.587.9797 | Benelux +31 (347) 324989

France +33 (1) 60.86.03.65 | Germany +49 (0) 89.660.779.3

Japan +81.3.5639.2741 | UK +44 (0) 2838.3101.71

...SEE the Future

Seya monochromator, where concave mirrors were positioned both before and after the entrance and exit slits. A further feature of the Wadsworth is that, unlike the Seya, it has no entrance slit, so this monochromator makes efficient use of the full horizontal aperture of the SR source. The instrument operates in horizontal dispersion, so its resolution is limited by the horizontal electron beam size in the storage ring, FWHM (full width at half maximum) *ca* 1.8 mm in the case of the Daresbury SRS, corresponding to a best resolution of *ca* 0.05 nm. This resolution would improve by a factor of *ca* five on a smaller-fan, third-generation source such as Diamond. The scanning mechanism uses an off-axis pivot which makes an approximate correction for the changing focus of the grating for different wavelengths. The length of the pivot arm can be varied externally to the vacuum, and different wavelength ranges can be covered without substantial loss in resolution. The position of the exit slit, i.e. the grating to exit slit distance, GS (Figure 1), can also be changed externally, allowing further optimisation of the resolution. Two gratings are mounted, interchangeable under vacuum, giving a wide range of wavelength coverage, currently *ca* 40–200 nm. The monochromator is preceded by a water-cooled metal plane

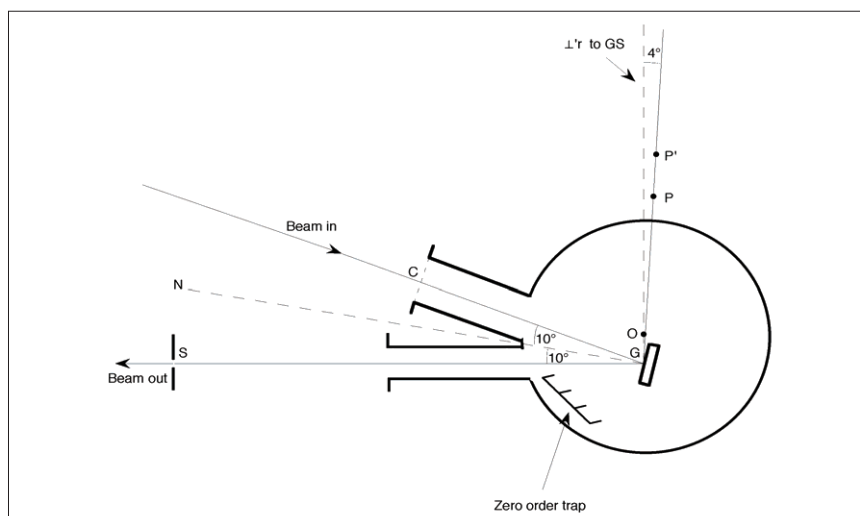


Figure 1. The new monochromator of Wadsworth design. G—diffraction grating; S—exit slit; C—centre of entrance flange where collimating baffles are fitted; O—vacuum chamber centre; P—pivot point, movable between P and P'. [Reproduced by permission from *Nucl. Instr. Methods B* 237, 656–665 (2005).]

mirror, which deflects the incident radiation through 20° onto the diffraction grating. The gratings scan about the pivot point which can be varied between P and P'. The 4° offset shown minimises the change in direction of the output beam, $\pm 0.04^\circ$, as the grating moves. A four-way cross fitted to the exit slit of the monochromator incorporates a retractable LiF window for rejection of higher orders when operating with $\lambda > 105$ nm, and

a retractable Si photodiode for absolute flux measurements. Absolute fluxes from the two gratings are better than 50% of the calculated values.¹ Furthermore, the experimental fluxes are over two orders of magnitude greater than that available from the old Seya monochromator operating at the same resolution. The cross is attached to a post-monochromator mirror chamber, which contains an elliptical and a plane mirror, thereby focusing

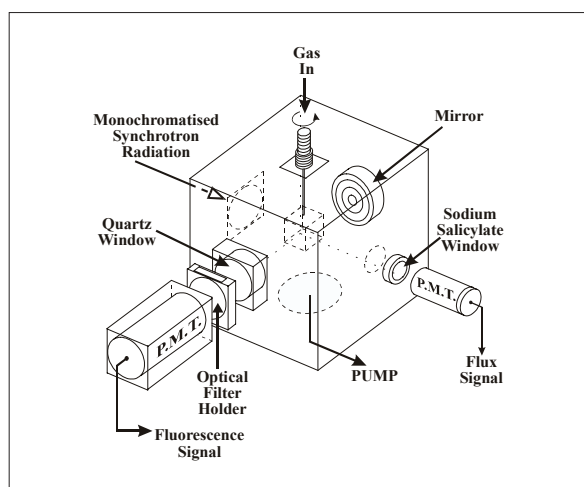


Figure 2. Schematic of the apparatus used for undispersed fluorescence excitation spectroscopy at Daresbury. [Reproduced by permission from *J. Elec. Spec. Rel. Phen.* 101–103, 101–107 (1999).]

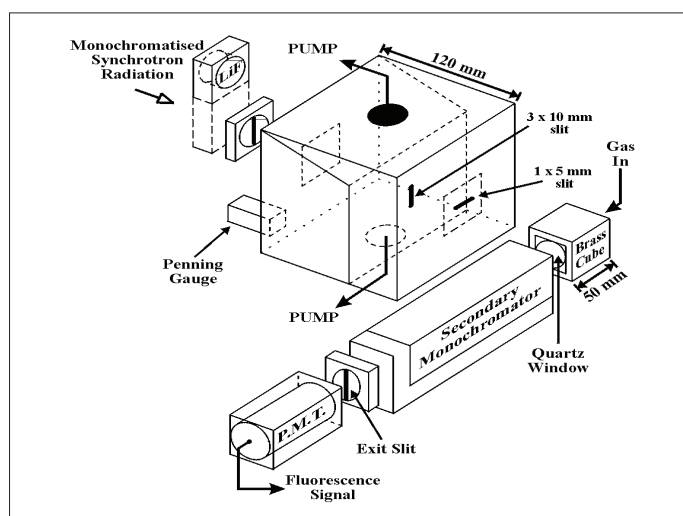


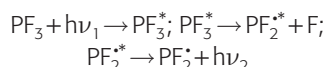
Figure 3. Schematic of the dispersed fluorescence apparatus used both at the Bessy I, Berlin and Daresbury SR sources. At Daresbury, the dispersing secondary monochromator is replaced by a liquid-N₂-cooled, multi-channel CCD detector. [Reproduced by permission from *J. Elec. Spec. Rel. Phen.* 101–103, 101–107 (1999).]

the exit slit with 1:1 demagnification at the centre of an exit flange. A capillary light guide is mounted on the exit flange to deliver the light efficiently to the experimental sample.

Vacuum-UV undispersed and dispersed fluorescence spectroscopy

The vacuum-UV spectroscopy of PF_3 using fluorescence excitation and dispersed emission techniques have been studied at the Daresbury and BESSY 1 SR sources.² The apparatus for such experiments are shown in Figures 2 and 3. The fluorescence excitation spectrum in the range 9–20 eV with an average resolution of ≈ 0.015 eV [Figure 4(a)] shows transitions to the three lowest Rydberg states with resolved vibrational structure. They are assigned to transitions to the $(8a_1)^{-1}4p$, $5p$ and $6p$ Rydberg states of

PF_3 , and fluorescence is due to valence transitions in the PF_2^{\cdot} free radical, i.e.



From a Franck–Condon analysis of the vibrational structure [Figure 4(b)], the FPF bond angle in PF_3 is shown to increase by $14 \pm 1^\circ$ upon photoexcitation. The bond angle of the Rydberg states of PF_3 is therefore $\approx 112 \pm 1^\circ$, and these states, and the ground state of PF_3^+ to which they converge, retain pyramidal C_{3v} symmetry. The use of optical filters, not shown in Figure 4(a), shows that at least three excited states of PF_2^{\cdot} are responsible for the emission. Dispersed emission spectra in the UV/visible have been recorded at BESSY 1,² and more recently at Daresbury (Figure 5) using a multi-channel CCD detector (Figure 3), giving detailed information on the electronic spectroscopy of the PF_2^{\cdot} radical.

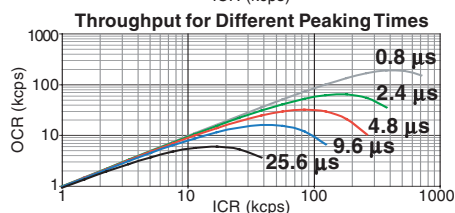
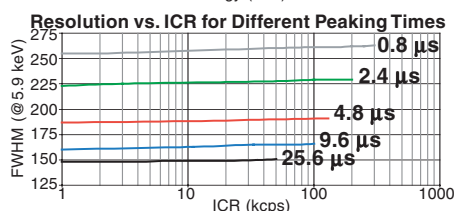
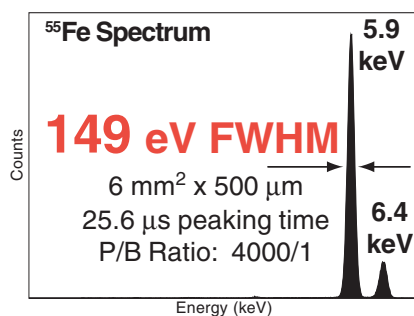
This work remains the most comprehensive study of the electronic spectroscopy of the PF_2^{\cdot} free radical. In part, this arises due to the clean method, vacuum-UV photodissociation of a stable precursor molecule, of generating the radical.

Threshold photoelectron photoion coincidence spectroscopy: application to SF_5CF_3

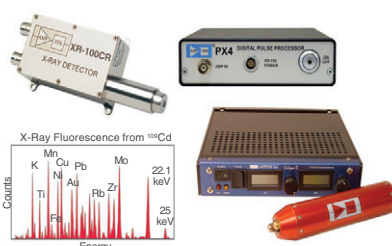
A recent paper described the infrared absorption spectrum of a potent greenhouse gas, SF_5CF_3 , and its detection in the earth's atmosphere.³ This molecule is an adduct of the SF_5^{\cdot} and CF_3^{\cdot} free radicals, and its origin is anthropogenic. Almost certainly, its source is the reaction of SF_5^{\cdot} , a breakdown product of the dielectric SF_6 in high voltage equipment, with CF_3^{\cdot} radicals on the surface of fluoropolymers. Firm measurements made in Antarctica of air samples pumped out

X-Ray Detector

XR-100CR

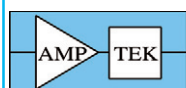


No Liquid Nitrogen!!
Low Cost
Solid State Design
Easy to Use



Complete XRF System
 XR-100CR X-Ray Detector
 PX4 Digital Pulse Processor, Power Supply, Shaping Amplifier and MCA
 ECLIPSE-III Portable X-Ray Tube System
 XRF-FP Quantitative Analysis Software

OEM's #1 Choice



AMPTEK Inc. 6 De Angelo Drive, Bedford, MA 01730-2204 USA
 Tel: +1 781 275-2242 Fax: +1 781 275-3470
 E-mail: sales@amptek.com www.amptek.com

Complete X-Ray Spectrometer

NEW!!!!



2.7 x 3.9 x 1 in. (7 x 10 x 2.5 cm)

The X-123 is a complete X-Ray Detector System in one small box that fits in your hand.

Features of the X-123:

- Simple to Operate
- Low Power (1.2 Watts)
- Small Size
- USB and RS232 Communication
- Accommodates all Types of Amptek Detectors

FASTLINK / CIRCLE 012 FOR FURTHER INFORMATION

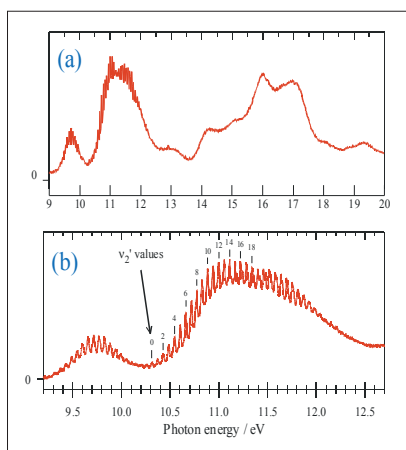


Figure 4. (a) Undispersed fluorescence excitation spectra of PF_3 between 9 and 20 eV recorded at the Daresbury SRS with the 5 m McPherson monochromator at a resolution of 0.1 nm, equivalent to a resolution of *ca* 0.01 eV at 12 eV. The effective range over which fluorescence is collected is 190–650 nm. (b) Expansion of (a) between 9.2 and 12.7 eV. The assignment of the transitions to ν_2' values of the $(8a_1)^{-1}5p$ Rydberg state of PF_3 is shown. A Franck–Condon analysis of the intensity distribution of these bands determine that the FPF bond angle increases by $14 \pm 1^\circ$ upon photoexcitation. [Reproduced by permission from *J. Chem. Phys.* **108**, 857–868 (1998).]

of consolidated snow suggested that the concentration of SF_5CF_3 at the end of the 20th century was still very small, *ca* 0.12 parts per trillion or 3×10^6 mole-

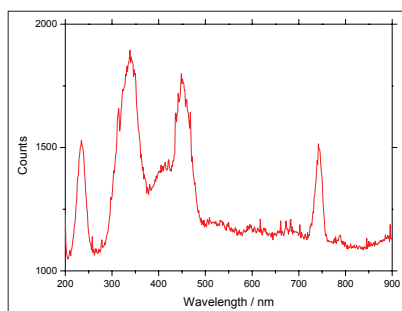


Figure 5. Dispersed spectra from PF_3 photoexcited at 14.4 eV, recorded at Daresbury using the new Wadsworth monochromator and the cooled CCD detector. Bands are due to electronic transitions in the PF_2 free radical. Assignments of the stronger bands are given in *J. Chem. Phys.* **108**, 857–868 (1998).

cules cm^{-3} , but it was growing at the huge rate of 6% per annum. As important, the strength of the infrared bands suggested that SF_5CF_3 has the strongest radiative forcing, *per molecule*, of any pollutant yet found in the earth's atmosphere. Small problems can become big problems in atmospheric chemistry, and this paper caused an explosion of interest world-wide to study the properties of this unusual molecule, especially those that affect its role in the earth's atmosphere. Chemists were particularly interested in the possible sink routes of this molecule from the atmosphere. Could UV photolysis in the stratosphere (15–50 km), the

principle cause of ozone depletion by chlorofluorocarbons, remove SF_5CF_3 ? Or was the S–C σ bond strong enough that SF_5CF_3 survived in the stratosphere, and it was removed at greater altitudes by processes in the mesosphere?

Using tunable vacuum-UV radiation in the range 12–25 eV from the old Seya–Namioka monochromator at Daresbury, we measured the threshold photoelectron–photoion coincidence (TPEPICO) spectrum of SF_5CF_3 , and determined indirectly the strength of the S–C bond in the neutral molecule.⁴ The apparatus (Figure 6) incorporates a threshold electron analyser, a linear time-of-flight mass spectrometer, a sodium salicylate window for flux normalisation, and software that allow TPEPICO spectra to be recorded continuously as a function of photon energy. Like CF_4^+ and SF_6^+ , the ground state of SF_5CF_3^+ is repulsive in the Franck–Condon region along the S–C coordinate. The onset of ionisation can therefore only give an upper limit to the energy of the first dissociative ionisation pathway of SF_5CF_3 to $\text{CF}_3^+ + \text{SF}_5 + e^-$. We have therefore determined the kinetic energy released into the two molecular fragments over a range of photon energies in the Franck–Condon region; the raw data for $\text{CF}_4 \rightarrow \text{CF}_3^+ + \text{F} + e^-$ is shown as a three-dimensional false colour map in Figure 7. Using an impulsive model

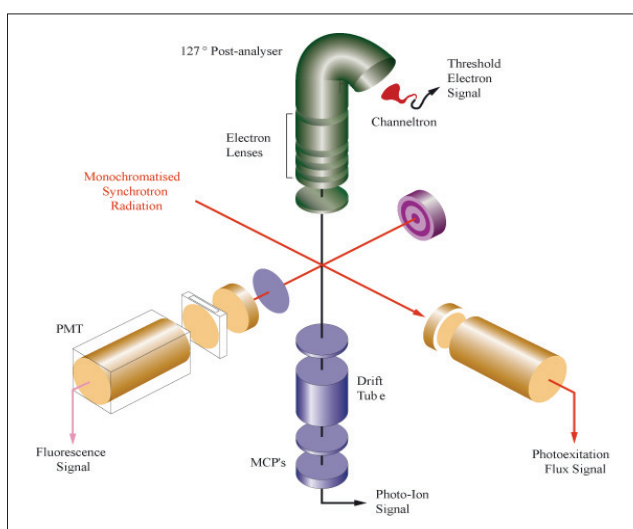


Figure 6. Schematic of the coincidence apparatus used to record threshold photoelectron photoion coincidence spectra as a function of vacuum-UV photon energy at the Daresbury SRS.

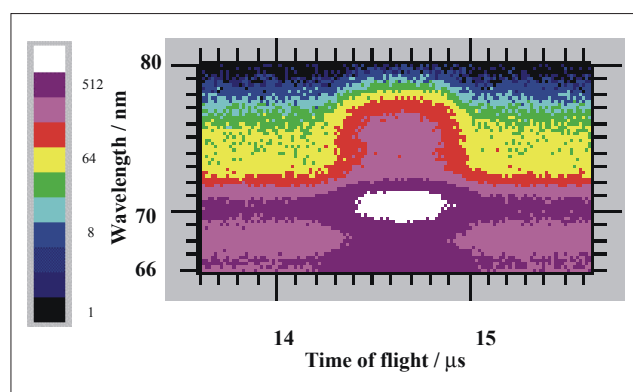


Figure 7. False-colour three-dimensional map of fragmentation of $\text{CF}_4 \rightarrow \text{CF}_3^+ + \text{F} + e^-$ between 66 and 80 nm (15.5 and 18.8 eV). Colour is shown on a logarithmic scale. The width of the CF_3^+ signal, centred at $14.65 \mu\text{s}$, for each wavelength channels is related to the translational kinetic energy release into the CF_3^+ and F fragments. A similar figure was obtained for fragmentation of $\text{SF}_5\text{CF}_3 \rightarrow \text{CF}_3^+ + \text{SF}_5 + e^-$ over the energy range of the Franck–Condon region of the electronic ground state of SF_5CF_3^+ .

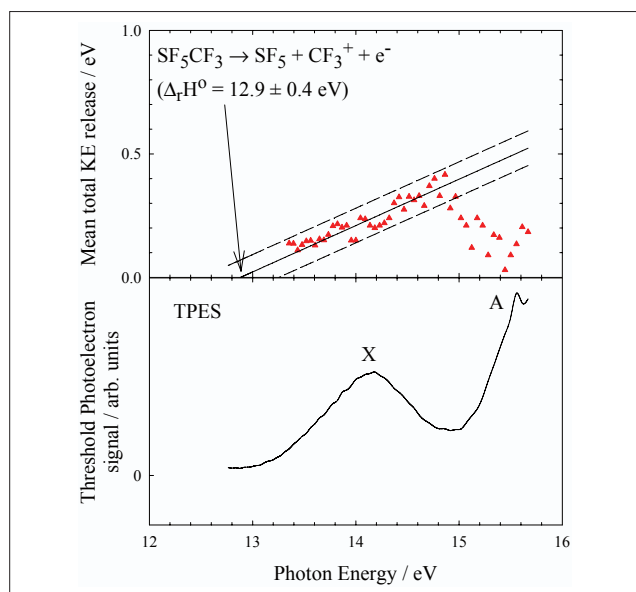


Figure 8. (a) Mean total kinetic energy released in the reaction $\text{SF}_5\text{CF}_3 + h\nu \rightarrow \text{CF}_3^+ + \text{SF}_5 + \text{e}^-$ for photon energies in the range 13.3–15.5 eV. A linear extrapolation to zero kinetic energy gives the first dissociative ionisation energy of SF_5CF_3 to be 12.9 ± 0.4 eV. We can then obtain values for the dissociation energy of the $\text{SF}_5\text{--CF}_3$ bond, 3.86 ± 0.45 eV, and the 0K enthalpy of formation of SF_5CF_3 , -1750 kJ mol $^{-1}$. (b) Threshold photoelectron spectrum (TPES) of SF_5CF_3 over the range 12.8–15.6 eV. [Reproduced by permission from *J. Phys. Chem. A*, **105**, 8403–8412 (2001).]

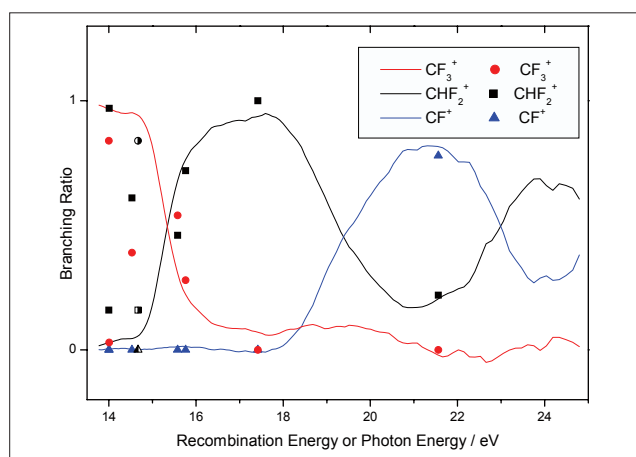


Figure 9. Comparison of the branching ratios for products from the ion–molecule reactions of CHF_3 with photoionisation branching ratios from threshold photoelectron photoion coincidence spectroscopy. The half-filled symbols at 14.67 eV correspond to Kr^+ in its excited $^2\text{P}_{1/2}$ spin-orbit component.

for photodissociation, the data for SF_5CF_3 has been analysed and extrapolated to zero kinetic energy. In this way, we determined experimentally the first dissociative ionisation energy for SF_5CF_3 to be 12.9 ± 0.4 eV (Figure 8). Subtracting the adiabatic ionisation energy of the CF_3^+ radical, 9.04 ± 0.04 eV, we obtained $D_0^0(\text{SF}_5\text{--CF}_3)$ of 3.86 ± 0.44 eV or 372 ± 42 kJ mol $^{-1}$.¹⁵ The atmospheric significance of this value is that the S–C bond is strong,



Missed

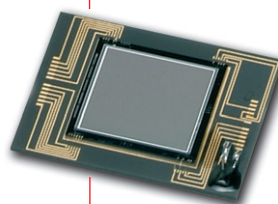
the Details?

CCD and CMOS Sensor Technology from Hamamatsu helps you to discover the hidden details in your applications.

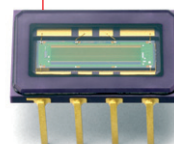
We are continually pushing the boundaries in CCD/CMOS design, manufacturing and unique packaging technologies.

Our world-leading production facilities have state-of-the-art manufacturing equipment and our continual improvement of these processes assures you of the highest level of product and service quality.

Today, we can provide tomorrow's leading edge CCD and CMOS Sensor technology and offer a wide variety of both standard and custom-made products.



S9737-03
Wide dynamic range megapixel CCD
for Scientific Applications
on a new plate package



S9227
5MHz Linear CMOS Sensor
with shutter function and
integrated Timing generator

HAMAMATSU

PHOTON IS OUR BUSINESS

Freephone:
Europe 00 800 800 800 88
USA 1-800 524 0504
www.sales.hamamatsu.com

and it is highly unlikely that SF_5CF_3 will be broken down by UV photolysis (200–400 nm) in the stratosphere. Subsequent (non-synchrotron) experiments showed that low-energy electron attachment in the mesosphere is the predominant process that removes this molecule from the earth's atmosphere. Its lifetime, however, is determined primarily by the slow processes, such as convection and diffusion, that transport this molecule up into the mesosphere. The best estimate is that the lifetime of SF_5CF_3 is as long as *ca* 1000 years. We are stuck with this potential environmental problem for the foreseeable future!

The role of long-range charge transfer in cation–molecule reactions: application to CHF_3

Fluoroform, CHF_3 , is a major industrial gas that is used as a feedgas in technological plasmas. Charged species are prevalent in such plasmas, and we have studied the room temperature kinetics and products of small cations, with recombination energies (*RE*) spanning the range *ca* 6–22 eV, reacting with CHF_3 in a selected ion flow tube.⁶ An additional motivation for such studies was to understand the importance of long-range charge transfer in ion–molecule reactions. We consider a cation (A^+) reacting with a neutral molecule (BC), where BC has a permanent dipole moment. Charge transfer can occur either at long range or at short range. In the long-range mechanism, A^+ and BC approach under the influence of their charge–dipole interaction, until the A^+ –BC and A – BC^+ potential energy curves cross. An electron jump can then take place. Two factors for rapid electron transfer are a non-zero energy resonance connecting BC to an electronic state of BC^+ at the *RE* of A^+ , and the transferring electron comes from a molecular orbital of BC that is not shielded from the approaching cation. The magnitude of the photoionisation Franck–Condon factor for BC is probably not important in determining the efficiency of such a reaction. We note that if this long-range charge transfer mechanism operates, then the branching ratios for fragmentation of $(\text{BC}^+)^*$, where (*) denotes the

possibility of BC^+ being in an excited electronic state, are expected to be independent of how this state is produced. Hence, we would expect similar product branching ratios from the ion–molecule study and from a TPEPICO photoionisation study, assuming the photon energy in the latter experiment matches the *RE* of A^+ in the former.

If long-range charge transfer does not happen, A^+ and BC move closer together, and distortion of the potential energy surface of interaction occurs. Eventually, a curve crossing can occur through which charge transfer takes place. This is called short-range charge transfer. As an intermediate complex has formed, a chemical reaction, defined as the breaking and making of new bonds, may, in addition, compete with short-range charge transfer. This means that it is unlikely that the product branching ratios from the ion–molecule and TPEPICO experiments will mimic each other. Thus, a comparison of the fragmentation patterns from the selected ion flow tube and TPEPICO experiments, together with an analysis of the threshold photoelectron spectrum of BC at the energy of the *RE* of A^+ , may indicate which mechanism, be it long-range or short-range, is dominant for the reaction of each cation.

The ionisation energy of CHF_3 is 13.85 eV, so only those ion–molecule reactions with $\text{RE}(\text{ion}) > 13.85$ eV need be considered. Figure 9 shows a comparison of the branching ratios for the two experiments. The data suggest that long-range charge transfer probably occurs for the Ar^+ and F^+ atomic ions whose recombination energies lie above *ca* 15 eV. The data for N_2^+ (*RE* = 15.58 eV) and Ar^+ (*RE* = 15.76 eV) are particularly surprising. Despite only a small difference between their *RE*s, the branching ratios from the two experiments in the selected ion flow tube are very different. We are unable to explain this surprising result, other than state the obvious that N_2^+ is molecular whereas Ar^+ is atomic. Below 15 eV, agreement between the branching ratios for the two experiments is poor, and the mechanism must involve a combination of short-range charge transfer and chemical reactions involving a transition state intermediate.

Conclusions and acknowledgments

In this article I have highlighted four areas of research where the use of tunable SR radiation in the vacuum-UV has led to important discoveries. These studies have exploited the tunability of such sources, albeit at moderate resolution. Other areas of research in gas-phase chemical physics use the polarisation properties of SR, and this is likely to be a growth area for research with the increasing availability of third-generation sources, with their ability to generate circularly polarised radiation. Studies on the ionisation properties of chiral molecules, for example, are then possible. Early results suggest that the measurement of photoelectron angular distributions using circularly polarised radiation could provide a sensitive, analytical sensor for the chiral form of such molecules.⁷

I thank past and present members of my research group who have contributed enormously to my efforts over the last 10–15 years. Financial support from the EPSRC and CCLRC research councils, the EU and the British Council is also acknowledged.

References

1. C.R. Howle, S. Ali, R.P. Tuckett, D.A. Shaw and J.B. West, *Nucl. Instr. Methods B* **237**, 656 (2005)
2. H. Biehl, K.J. Boyle, D.P. Seccombe, R.P. Tuckett, H. Baumgärtel and H.W. Jochims, *J. Chem. Phys.* **108**, 857 (1998).
3. W.T. Sturges *et al.*, *Science* **289**, 611 (2000).
4. R.Y.L. Chim, R.A. Kennedy, R.P. Tuckett, W. Zhou, G.K. Jarvis, D.J. Collins and P.A. Hatherly, *J. Phys. Chem. A* **105**, 8403 (2001).
5. R.P. Tuckett, *Adv. Fluorine Science*, Volume 1, Ed by A. Tressaud. Elsevier, in press (2006).
6. M.A. Parkes, R.Y.L. Chim, C.A. Mayhew, V. Mikhailov and R.P. Tuckett, *Mol. Phys.*, in press (2005).
7. U. Hergenbahn, E.E. Rennie, O. Kugeler, S. Marburger, T. Lischke, I. Powis and G. Garcia, *J. Chem. Phys.* **120**, 4553 (2004).